Macromolecules

pubs.acs.org/Macromolecules Article

Synergy between Ionic Capacity and Intrinsic Porosity in Imidazolium-Based Cationic Organic Polymers and Its Effect on Anionic Dye Adsorption

Shu-Qing Fu, Ming-Zhi Zhu, Boxin Xue,* and Pei-Nian Liu*

Cite This: *Macromolecules* 2022, 55, 8784–8794 Read Online

ACCESS | Metrics & More | Article Recommendations | Supporting Information

ABSTRACT: A series of novel imidazolium-based cationic organic polymers (COPs) with various ionic capacities (ICs) and porosities were synthesized by adjusting the structure of the building units and applied to the adsorption of organic dyes from aqueous solutions. The charge-incorporated polymer without pores was almost incapable of adsorbing dyes. Among polymers with similar porosities, COPs with higher IC values exhibited higher adsorption capacities, and the polymer with the largest IC but only a surface area of 74.2 $m^2\ g^{-1}$ exhibited the best adsorption performance toward Acid Orange 7 (559.4 mg g^{-1}, 21 times that of the uncharged polymer). The results demonstrated the synergistic effect between IC and intrinsic porosity: high porosity was necessary for adsorption, whereas electrostatic interactions between charges and dyes dominate removal efficiency; increasing the charge content is more effective than increasing the surface area in this polymer system. This work provides in-depth insight into the organic-dye adsorption process and a path toward the rational molecular design of high-performance COPs.

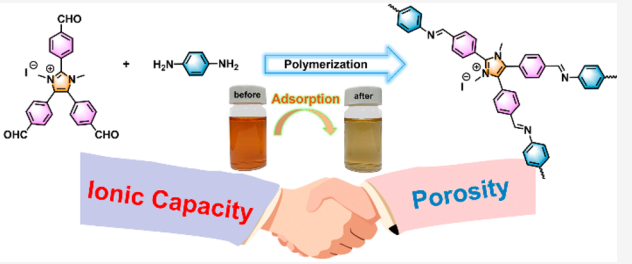

INTRODUCTION

Water pollution is an environmental issue of significant public concern.[1−3] Organic dyes are the most common wastewater pollutants and are released during textile, clothing production, printing, and dyeing processes, greatly threatening both human health and the ecosystem.[4−6] In recent years, various porous materials have been reported as effective adsorbents for dye removal,[7−9] and the task-specific design and construction of porous organic polymers (POPs) have been proposed as promising solutions for tackling dye pollution issues. POPs are fabricated by the formation of strong covalent bonds between light elements and have clear advantages, including large specific surface areas, good thermal stabilities, and excellent chemical stabilities.[8,10−15] Moreover, POPs are easily prepared by Pd-catalyzed coupling,[8,16−20] Friedel−Crafts,[21−26] Menshutkin,[27−31] or Schiff-base reactions.[12,32−36] Most importantly, their pore properties are tunable and designable, which enables POPs to be designed in a task-specific manner based on the molecular characteristics of the dye.[37]

Initially, most reported POPs were neutral and did not contain specific functional groups; these adsorbents required high porosities to provide sufficiently high numbers of available adsorption sites, thereby ensuring high capacities for dye adsorption.[38] For example, Tan et al. reported the polymerization of commercial triptycene monomer using low-cost Friedel−Crafts reaction. A triptycene-based hyper-cross-linked POP with a surface area of up to 1426 $m^2\ g^{-1}$ was successfully synthesized, and highly efficient adsorption for Congo Red (CR, 1537 mg g^{-1}), Methyl Blue (MB^{2-}, 787 mg g^{-1}), and Methylene Blue (MLB^+, 330 mg g^{-1}) was achieved.[26] Chen et al. synthesized a POP (**CMP-YA**) through transition-metal-catalyzed Yamamoto coupling polymerization. With a high surface area of 1410 $m^2\ g^{-1}$ and microporous structure, **CMP-YA** exhibited excellent adsorption capacities of CO_2 and organic dyes, and the maximum adsorption capacity of MLB^+ in water reached up to 1016 mg g^{-1}, higher than most of the reported adsorbents.[9] The dye-adsorbing functions of such POPs depend mainly on pores and are driven by van der Waals forces.[28,39,40]

Enhancing adsorbent/adsorbate interactions is another important strategy for improving the dye-adsorption capacities of POPs. Cationic organic polymers (COPs) with positive charges incorporated in their skeletons represent a small fraction of the POP family and have been much less explored than neutral POPs.[28,31,41−43] For example, Han et al. reported an imidazolium-based COP that selectively captures anionic pollutants with high capacities, excellent selectivities, and fast kinetics.[12,44] The pyridinium-based COPs developed by Ma et al. are reportedly ideal ReO_4^-/TcO_4^- scavengers with optimal

Received: May 31, 2022
Revised: August 26, 2022
Published: September 22, 2022

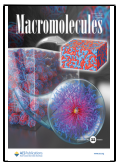

https://doi.org/10.1021/acs.macromol.2c01127
Macromolecules 2022, 55, 8784−8794

Scheme 1. Synthesis Routes of (a) the Monomers (MITT and TFDI) and (b) the Imidazolium-Based COPs (IMP-1, IMP-2, IMP-3, IMP-4, and IMP-5) and Uncharged Polymer U-IMP-6 via the Schiff Base Reaction and the Pictures of IMPs Powder (from Left to Right: IMP-1, IMP-2, IMP-3, IMP-4, IMP-5, and U-IMP-6)

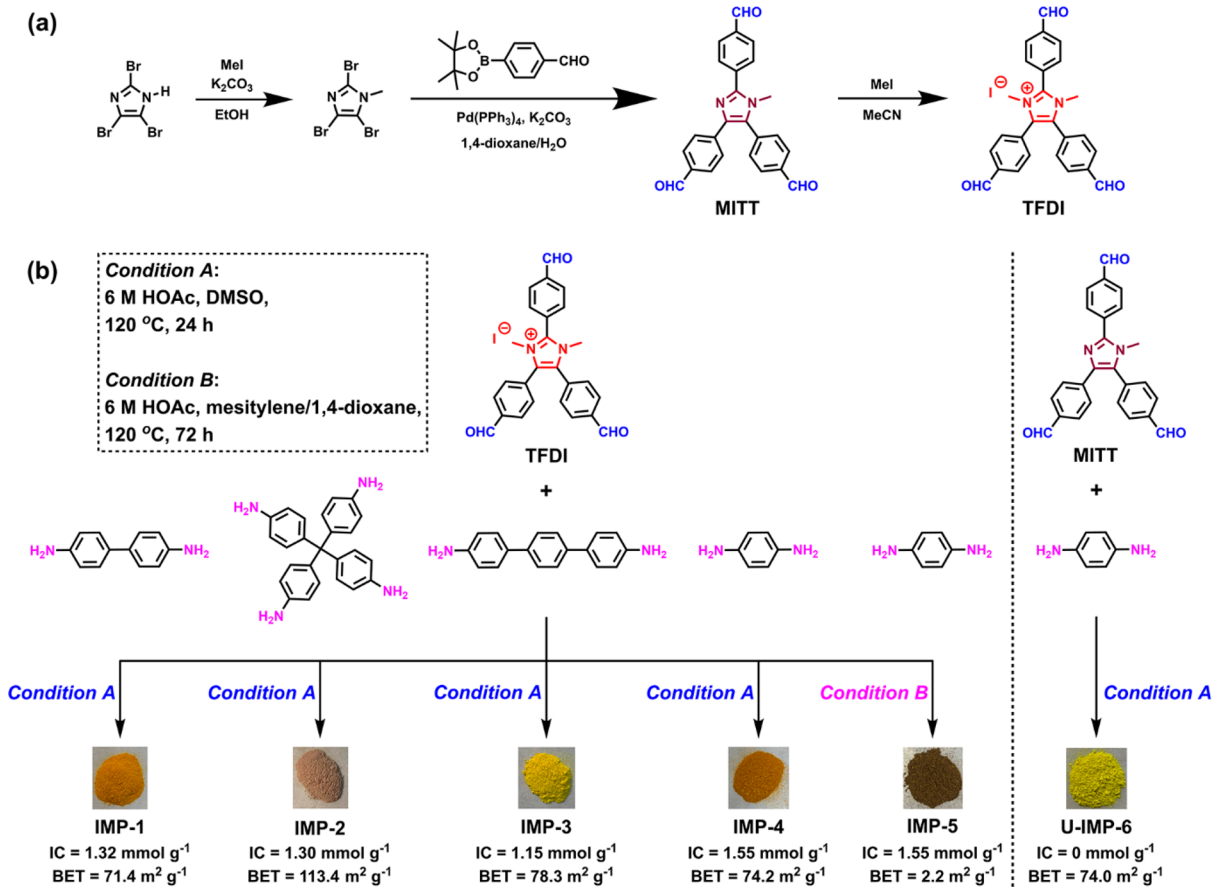

uptake capacities and selectivities.[15] Qiu et al. synthesized a chemically stable imidazolium-based COP; its densely accessible cationic sites led to a large adsorption capacity and fast kinetics for ReO_4^-.[28] Ma et al. used the Menshutkin reaction to construct a COP that was shown to exhibit a dual capturing capability for both oxo anions and anionic organic dyes.[37] Given the abundant charges within the COPs, strong electrostatic interactions between an anionic pollutant and the COP greatly promote adsorption kinetics, resulting in the efficient and selective removal of various anionic pollutants. While ionic capacity (IC, the ion content per unit mass) is an important COP parameter, its effect on the effectiveness of adsorption for organic dyes has not been explored yet, despite being greatly significant for understanding the adsorption process in depth and the rational molecular design of high-performance COPs.

Herein, we developed a series of novel imidazolium-based COPs (**IMP-1−5**) and a neutral uncharged polymer (**U-IMP-6**) using a direct Schiff-base polymerization reaction, with IC and porosity regulated by adjusting the structures of the building units (Scheme 1). Adsorption experiments were performed to determine the ability of each adsorbent to remove various dyes from aqueous solutions. The charge-incorporated polymer devoid of pores was found to be almost incapable of adsorbing dyes. Among polymers with similar porosities, COPs with higher IC values exhibited higher adsorption capacities. Impressively, the polymer with the largest IC but only a surface area of 74.2 $m^2\ g^{-1}$ exhibited the best adsorption performance toward anionic dyes. These findings reveal the important synergistic effect between IC and intrinsic porosity of the adsorbent; that is, while porosity is necessary, strong electrostatic interactions between the polymer charges and the dye play dominant roles in removing the anionic dye, and increasing the charge content is more effective than increasing the surface area in this polymer system.

EXPERIMENTAL SECTION

Materials. Mesitylene, 1,4-dioxane, 1,2-dichlorobenzene (*o*-DCB), 1-butanol (*n*-BuOH), dimethyl sulfoxide (DMSO), acetic acid (HOAc), dichloromethane (DCM), *N*,*N*-dimethylformamide (DMF), tetrahydrofuran (THF), acetone, ethanol (EtOH), methanol (MeOH), acetonitrile, sodium chloride (NaCl), potassium carbonate (K_2CO_3), and sodium sulfate (Na_2SO_4) were purchased from Shanghai Chemical Works, China. *p*-Phenylenediamine, benzidine, 4,4″-diamino-*p*-terphenyl, tetrakis(4-aminophenyl)methane, iodomethane (MeI), 2,4,5-tribromoimidazole, 4-(4,4,5,5-tetramethyl-1,3,2-dioxaborolan-2-yl)benzaldehyde, and tetrakis(triphenylphosphine) palladium ($Pd(PPh_3)_4$) were purchased from Aladdin. Acid Orange 7 ($AO7^-$), Methyl Blue (MB^{2-}), Amaranth (AMR^{3-}), and Methylene Blue (MLB^+) were purchased from Macklin. All chemicals were used as received without any purification. 2,4,5-Tribromo-1-methyl-1*H*-imidazole was synthesized according to a literature method.[45]

Measurements. All Fourier transform infrared (FTIR) spectra were detected by using a Nicolet is50 spectrometer using KBr pellets in a range of 400−4000 cm^{-1}. Solid-state ^{13}C cross-polarization magic angle spinning (CP/MAS) nuclear magnetic resonance (NMR) measurements were performed on an Agilent-NMR-vnmrs-600

https://doi.org/10.1021/acs.macromol.2c01127
Macromolecules 2022, 55, 8784−8794

spectrometer. Chemical shifts (δ, ppm) in the ^{1}H NMR spectra were recorded using TMS as internal standard or internally referenced to $CDCl_3$ (δ = 7.26 ppm), while the ^{13}C NMR spectra were internally $CDCl_3$ (δ = 77.0 ppm). HRMS data were obtained using ESI-TOF (electrospray ionization time-of-flight) or using EI-TOF (electron ionization time-of-flight) on a Waters GCT Premier mass spectrometer. Melting points were determined in opened capillary tubes and uncorrected. The porosities of the materials were determined by nitrogen adsorption−desorption experiment that was conducted at 77.3 K on a ASAP2460 instrument. Samples were vacuumed at 120 °C for 8 h before the sorption analysis. Powder X-ray diffraction (PXRD) patterns were recorded in a range of 2θ = 3°−50° on a desktop X-ray diffractometer (18KW/D/max2550VB/PC) with Cu Kα radiation (λ = 1.5406 Å) at room temperature. Scanning electron microscopy (SEM) image and energy dispersive spectrometry (EDS) elemental mapping were obtained from a Hitachi field-emission scanning electron microscope (S-4800) with an electric voltage of 5 kV. Transmission electron microscopy (TEM) images were observed on a JEOL JEM 2100F microscope. The chemical compositions of the obtained materials were evaluated by X-ray photoelectron spectroscopy (XPS, Thermo Scientific ESCALAB Xi+). The thermal properties of the products were characterized by thermogravimetric analysis (TGA) and derivative thermogravimetry (DTG) on a TGA 8000 at a heating rate of 10 °C min^{-1} from 35 to 800 °C under nitrogen flow. Ultraviolet−visible (UV−vis) spectra were recorded on a UV-6100 spectrophotometer (METASH, China) and used to determine the concentration of dyes.

Synthesis of 4,4′,4″-(1-Methyl-1*H*-imidazole-2,4,5-triyl)-tribenzaldehyde (MITT) and 2,4,5-Tris(4-formylphenyl)-1,3-dimethyl-1*H*-imidazol-3-ium (TFDI). *4,4′,4″-(1-Methyl-1H-imidazole-2,4,5-triyl)tribenzaldehyde (**MITT**).* The stirred solution of 2,4,5-tribromo-1-methyl-1*H*-imidazole(1.0 g, 3.1 mmol), 4-(4,4,5,5-tetramethyl-1,3,2-dioxaborolan-2-yl)benzaldehyde (4.4 g, 18.8 mmol), $Pd(PPh_3)_4$ (181 mg, 0.16 mmol), and K_2CO_3 (2.6 g, 18.8 mmol) in 35 mL of 1,4-dioxane and 6 mL of water was heated to 100 °C under a nitrogen atmosphere. Stirring was continued overnight, and then the mixture was cooled to room temperature. Water was added, and organic compounds were extracted with dichloromethane three times. The combined organic phases were washed with the saturated aqueous sodium chloride solution (3 × 30 mL) and dried over Na_2SO_4, and the solvent was removed in vacuo. The crude solid was purified by a short column of silica gel and eluted with DCM:MeOH = 100:1 to afford **MITT** as a yellow solid (1.2 g, 98% yield). ^{1}H NMR (600 MHz, $CDCl_3$-*d*): δ 10.13 (s, 1H), 10.11 (s, 1H), 9.95 (s, 1H), 8.05 (m, 4H), 7.99 (d, *J* = 8.1 Hz, 2H), 7.76 (d, *J* = 8.3 Hz, 2H), 7.68 (d, *J* = 8.3 Hz, 2H), 7.62 (d, *J* = 8.0 Hz, 2H), 3.63 (s, 3H). ^{13}C NMR (151 MHz, $CDCl_3$-*d*): δ 191.80, 191.58, 191.38, 147.91, 139.75, 138.12, 136.58, 136.45, 136.06, 135.50, 134.89, 131.85, 131.33, 130.52, 130.04, 129.94, 129.49, 127.45, 33.84. HRMS (EI, TOF): calcd for [M]: 394.1317; found for [M]: 394.1321; melting point: 199−200 °C.

*2,4,5-Tris(4-formylphenyl)-1,3-dimethyl-1H-imidazol-3-ium (**TFDI**).* A solution of **MITT** (1.0 g, 2.5 mmol) and MeI (1.6 mL, 25.4 mmol) in 13 mL of acetonitrile was heated to reflux and stirred overnight. After cooling the mixture to room temperature, volatiles were evaporated. The crude solid was purified by a short column of silica gel and eluted with DCM:MeOH = 100:1 to afford **TFDI** as a brown solid (1.2 g, 85% yield). ^{1}H NMR (600 MHz, $CDCl_3$-*d*): δ 10.16 (s, 1H), 10.00 (s, 2H), 8.55 (d, *J* = 8.2 Hz, 2H), 8.13 (d, *J* = 8.3 Hz, 2H), 7.92 (d, *J* = 8.2 Hz, 4H), 7.82 (d, *J* = 8.3 Hz, 4H), 3.68 (s, 6H). ^{13}C NMR (151 MHz, $CDCl_3$-*d*): δ 191.32, 191.09, 144.15, 138.94, 137.33, 133.04, 132.30, 132.16, 130.78, 130.42, 130.00, 126.88, 35.30. HRMS (ESI, TOF): calcd for $[M - I]^+$: 409.1547; found for $[M - I]^+$: 409.1551; melting point: 155−157 °C.

Synthesis of Imidazolium-Based Cationic Organic Polymers (IMP-1−5) and Neutral Uncharged Polymer (U-IMP-6). *Synthesis of IMP-1.* **TFDI** (472.0 mg, 0.88 mmol) and benzidine (243.2 mg, 1.32 mmol) were dissolved in 11.0 mL of DMSO in a 25 mL glass vial by sonication until a clear solution formed. Then, 1.1 mL of 6 M HOAc was added as a catalyst, at which point the solution gelled within 1 min. The glass vial was further sealed using Teflon tape to prevent the solvent leakage during the heating process and stirred at 120 °C for 24 h to complete the reaction. After reacting for 24 h, all samples were cooled to room temperature; the reaction mixture was poured into DCM, and a bulk precipitate formed. The precipitate was filtered off, washed with DMF, THF, and acetone in sequence three time (50 mL for each), and then dried at 80 °C under vacuum overnight to give **IMP-1** as orange powder (yield: 77%; relative to the used amount of monomer).

IMP-2, **IMP-3**, and **IMP-4** were obtained using the same procedure, and tetrakis(4-aminophenyl)methane, 4,4″-diamino-*p*-terphenyl, and *p*-phenylenediamine were used as the amino monomers, respectively. The yields of **IMP-2** (pale purple powder), **IMP-3** (yellow powder), and **IMP-4** (orange powder) are 90, 70, and 76%, respectively.

*Synthesis of **IMP-5**.* A mixture of mesitylene/1,4-dioxane solvent (0.5 mL/0.5 mL), **TFDI** (42.9 mg, 0.08 mmol), *p*-phenylenediamine (13.0 mg, 0.12 mmol), and an aqueous HOAc solution (6 M, 0.1 mL) in a Pyrex tube (10 mL) was degassed by three freeze−pump−thaw cycles. The tube was sealed and stirred at 120 °C for 72 h. The precipitate was collected by filtration, washed with DMF, THF, and acetone in sequence three times (10 mL for each), and then dried at 80 °C under vacuum overnight to give **IMP-5** as dark brown powder (yield: 79%; relative to the used amount of monomer).

*Synthesis of **U-IMP-6**.* **MITT** (346.8 mg, 0.88 mmol) and *p*-phenylenediamine (142.7 mg, 1.32 mmol) were added to 11.0 mL of DMSO in a 25 mL glass vial. The mixed solution was sonicated for 3 min. Then, 1.1 mL of 6 M HOAc was added as a catalyst, at which point the solution formed suspension. The glass vial was further sealed using Teflon tape to prevent the solvent leakage during the heating process and stirred at 120 °C for 24 h to complete the reaction. When the reaction was completed, the mixed solution was poured into DCM, and the precipitate was collected by filtrating and washed successively with DMF, THF, and acetone. The yellow powder was dried via removing the residue solvents at 80 °C under vacuum overnight and collected with a yield of 78%.

Calculation of Ionic Capacity (IC). The ionic capacity (IC, mmol g^{-1}) of the imidazolium-based COPs is the ion content per unit mass which can be calculated from the number of ions per repeat unit of the imidazolium-based COPs according to the feeding proportion by the following equation[46]

$$IC = n/M \quad (1)$$

where M (g mol^{-1}) is the molar mass of the repeat unit of the imidazolium-based COPs and n (mmol mol^{-1}) is the molar cation content of the repeat unit of the imidazolium-based COPs.

Adsorption Experiments. *Procedures for the Dye Adsorption, Sorption Kinetics, and Sorption Isotherm Studies.* Two common types of dyes were selected for adsorption experiments, including negatively charged AO7$^-$, MB^{2-}, and AMR^{3-} and positively charged MLB$^+$. A series of adsorption experiments of these dyes were performed at 30 °C to evaluate the adsorbing capabilities of the imidazolium-based COPs for organic dyes in water. A typical AO7$^-$ adsorption experimental procedure for **IMP-4** was given as an example. For the adsorption kinetics experiments, the adsorption amounts at different times were tested in independent systems, and the standard procedure is as follows: 5 mg of **IMP-4** was weighed and placed in a 30 mL glass sample bottle, and then 25 mL of AO7$^-$solution (160 mg L^{-1}) was added. The absorbance of solutions with different adsorption times was monitored by liquid-phase UV−vis spectroscopy based on the typical absorption peak of AO7$^-$ at 484 nm. Additionally, the adsorption capacities of AO7$^-$ versus time were calculated from the time-dependent study (see sorption kinetics study in the Supporting Information). Moreover, the pseudo-first-order kinetic model and pseudo-second-order kinetic model were used for kinetics data of AO7$^-$ to be fitted in Table S4 and Figure 6b. To obtain the adsorption isotherm, the initial AO7$^-$ concentration was varied in the range from 0 to 265 mg L^{-1}. Thirty milligrams of **IMP-4** was added into each round-bottom flask containing 100 mL of AO7$^-$ solution. After stirring for 24 h, the AO7$^-$ concentration was

https://doi.org/10.1021/acs.macromol.2c01127
Macromolecules 2022, 55, 8784−8794

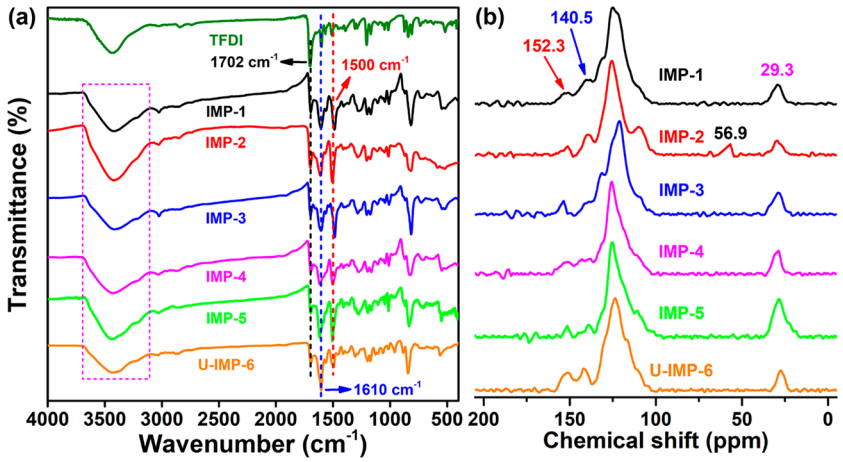

Figure 1. (a) FTIR spectra of **TFDI**, **IMP-1−5**, and **U-IMP-6**. (b) Solid-state ^{13}C NMR spectra of **IMP-1−5** and **U-IMP-6**.

determined by liquid-phase UV−vis spectroscopy. Additionally, the adsorption capacities of $AO7^-$ versus equilibrium concentration were calculated from the concentration-dependent study. Moreover, the Langmuir model and Freundlich model were used for isotherm data of $AO7^-$ to be fitted in Table S5 and Figure 6d. The adsorption of MB^{2-}, AMR^{3-}, and MLB^+ was measured in a similar way (the characteristic peaks of MB^{2-}, AMR^{3-}, and MLB^+ in the UV−vis spectra are 594, 521, and 664 nm, respectively).

Selective Adsorption. To study the adsorption of the target dye in the presence of interfering dyes, we selected the mixed dye solution of $AO7^-/MLB^+$ to conduct the separation test. **IMP-4** (30 mg) was dispersed in 100 mL of $AO7^-/MLB^+$ mixed dye solution, and the mixture was drastically stirred for 24 h. Finally, **IMP-4** solid particles were filtered off from the solution, and the liquid-phase UV−vis spectra of the filtrate were collected.

Recyclability Test. The recyclability of **IMP-4** was investigated by carrying out repeated adsorption and desorption steps using $AO7^-$ as a model dye. The **IMP-4** was regenerated with a mixed solution of MeOH and saturated NaCl aqueous in the ratio of 10:1 (v:v) until the filtrate was nearly colorless. Afterward, the solid was collected and dried at 80 °C under vacuum overnight. The dried **IMP-4** was recycled for the next run.

RESULTS AND DISCUSSION

A facile and cost-effective synthetic method that facilitates the development of ionic porous organic materials is crucial. For example, the Schiff-base reaction has been shown to be very useful for the construction of ionic porous polymers, and the design of the reaction monomer is the key to the success of this reaction. In this work, the uncharged 4,4′,4″-(1-methyl-1*H*-imidazole-2,4,5-triyl)tribenzaldehyde (**MITT**) imidazole-based trialdehyde monomer was constructed using Suzuki−Miyaura coupling chemistry, after which the 2,4,5-tris(4-formylphenyl)-1,3-dimethyl-1*H*-imidazol-3-ium (**TFDI**) imidazolium-based trialdehyde monomer was prepared by the simple quaternization of **MITT**, as illustrated in Scheme 1a. Their chemical structures were characterized and verified by ^{1}H NMR, ^{13}C NMR, and high-resolution mass spectra (Supporting Information).

The optimization of synthesis conditions are shown in Table S1. Polymers **IMP-1−4** were prepared by the reactions of **TFDI** and amino monomers with various molecular sizes under condition A in DMSO as the reaction solvent (Scheme 1b). **IMP-5** was formed in a similar manner to **IMP-4** but under condition B in a mixture of mesitylene and 1,4-dioxane as an alternative reaction solvent. In addition, **MITT** was reacted with *p*-phenylenediamine to give **U-IMP-6**, the uncharged polymer, for comparison. The ICs of **IMP-1−5** were calculated to be 1.32, 1.30, 1.15, 1.55, and 1.55 mmol g^{-1}, respectively, based on the number of ions per repeat unit. Because **U-IMP-6** has an uncharged framework, its IC is 0 mmol g^{-1}.

The chemical structures of **IMP-1−5** and **U-IMP-6** were characterized by FTIR and solid-state ^{13}C NMR spectroscopies (Figure 1). The FTIR spectrum of **TFDI** (Figure 1a) shows a characteristic carbonyl-stretching band at ∼1702 cm^{-1} (C═O); this band was significantly less intense after polymerization (Figure 1a), consistent with high aldehyde-group conversion. The band at around 1610 cm^{-1} is ascribable to overlapping C═C and C═N stretching vibrations, consistent with the formation of imine linkers in the imidazolium-based COPs. In addition, the band at ∼1500 cm^{-1} can be assigned to C═N stretching vibrations of imidazolyl rings, indicative of the presence of imidazolium or imidazole moieties. The polar imidazolium and imidazole moieties within the prepared polymers have high water uptake, so the broad peaks were observed around 3500 cm^{-1}, which were mainly ascribed to the stretching vibrations of −OH in water.

The solid-state ^{13}C NMR spectrum of each imidazolium-based COP (Figure 1b) shows a signal at ∼29.3 ppm that corresponds to methyl substituents on imidazolyl rings. The broad signal at 103.1−135.1 ppm is ascribable to overlapping phenyl- and imidazolyl-ring carbons, while the signal for the imidazolium carbon appears at ∼140.5 ppm. The presence of an imine peak at ∼152.3 ppm confirms that the imidazolium-based COPs had been successfully synthesized using Schiff-base chemistry. The peak at ∼56.9 ppm in the ^{13}C NMR spectrum of **IMP-2** corresponds to the central aliphatic carbon atom of the tetraarylmethane moiety.

Nitrogen adsorption−desorption isotherms and pore size distribution (PSD) curves of **IMP-1−4** and **U-IMP-6** were acquired to determine the porosities of **IMP-1−5** and **U-IMP-6**, the results of which are shown in Figures 2a and 2b, respectively. Brunauer−Emmett−Teller (BET) surface areas of 71.4, 113.4, 78.3, 74.2, 2.2, and 74.0 m^2 g^{-1} were calculated for **IMP-1−5** and **U-IMP-6**, respectively. We attribute the low BET specific surface areas of all COPs mainly to their structural characteristics. First, the monomers **TFDI** and **MITT** are not C3 symmetric molecules. The obtained amorphous and irregular structures may induce the collapse and blockage of the pores, thus resulting in a reduction in BET specific surface area. Second, during the polymer preparation,

https://doi.org/10.1021/acs.macromol.2c01127
Macromolecules 2022, 55, 8784−8794

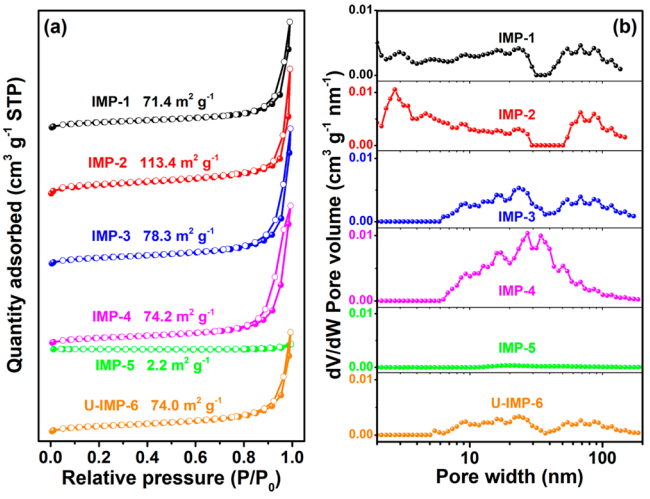

Figure 2. (a) Nitrogen adsorption−desorption isotherms at 77.3 K of **IMP-1−5** and **U-IMP-6** (the adsorption branches are labeled with filled symbols, and the desorption branches are labeled with empty symbols). (b) Pore size distribution curves of **IMP-1−5** and **U-IMP-6** via nonlocal density functional theory (NLDFT) calculation.

we found that the reactivities of **MITT** and **TFDI** were not high. Part of the aldehyde groups remained in the obtained polymer (as evidenced by the FTIR spectra in Figure 1a), so there would be a small amount of residue structure in the polymer network, leading to the formation of some macropores (>50 nm, as shown by the pore size distribution in Figure 2b). The macropores could lead to the low BET specific surface area values because the used BET calculation method does not refer to the macropore portion.

Among these polymers, **IMP-2** has the largest BET surface area, which is ascribable to its spatial three-dimensional structure. It should be mentioned that, apart from the reaction solvent, **IMP-4** and **IMP-5** were synthesized under the same conditions; however, the BET surface areas of **IMP-4** and **IMP-5** are significantly different (74.2 and 2.2 m^2 g^{-1}, respectively). The higher BET surface area of **IMP-4** is ascribable to the better solubility of the reactive monomers in DMSO than in mesitylene/1,4-dioxane during the Schiff-base reaction, which is favorable for porous-network formation. **TFDI** and *p*-phenylenediamine are only partially soluble in mesitylene/1,4-dioxane; hence, a heterogeneous reaction is formed that may lead to **IMP-5**/monomer coprecipitation. Moreover, the remaining insoluble monomers and oligomers tend to clog the pores of isolated material, resulting in a lower BET surface area.[47−49] Straight lines are displayed in the nitrogen adsorption−desorption isotherm and the pore-size distribution profile of **IMP-5**, confirming that it is devoid of pores. The uncharged **U-IMP-6** polymer has a BET surface area similar to that of **IMP-4**, which indicates that charge has no apparent effect on the porosity of the polymer. The nitrogen adsorption−desorption isotherms of **IMP-1−4** and **U-IMP-6** are combinations of types II and IV according to the IUPAC classification system.

The PSD profiles of **IMP-1−4** and **U-IMP-6** appear in the range of 2−200 nm, revealing hierarchical porous structures with meso- and macropores; their average pore diameters (D_{aver}) are determined to be 22.4, 16.8, 26.0, 28.0, 12.6, and 20.4 nm, respectively. The total pore volumes (V_{total}), estimated from the amount of N_2 adsorbed at P/P_0 = 0.99, are 0.40, 0.48, 0.51, 0.52, 0.01, and 0.38 cm^3 g^{-1}, respectively (Table 1). Generally, more small pores may result in more pore walls; hence, the BET specific surface area may be higher, while the pore volume may be smaller. These polymers all exhibit hierarchical porous structures, and their pore distributions are not identical, probably leading to different regularity between BET specific surface area and pore volume.

The thermal stability of the monomers and polymers was evaluated by TGA (Figure 3a) and DTG (Figure S1). The decomposition temperatures of **MITT** and **TFDI** are higher than 200 and 250 °C, respectively, confirming their excellent thermal stability. **IMP-1−5** exhibit similar thermal stability because of their similar structures, with each TGA curve exhibiting three distinct stages. The initial weight loss of the polymer observed below 180 °C is attributable to water and solvent-molecule volatilization, while the following two stages (200−500 °C) correspond to the decomposition of imidazolium cations and imine bonds; the final stage (∼500 °C) is attributable to backbone decomposition. In comparison, the uncharged imidazole-based **U-IMP-6** is stable to 400 °C, which is possibly due to the extremely high thermal stability of the uncharged imidazole moiety.

The crystallinities of the imidazolium-based COPs were investigated by PXRD. The PXRD profiles displayed in Figure 3b show broad robust peaks at ∼23°, indicative of the formation of amorphous phases in the imidazolium-based COPs in a similar manner to many reported COPs.[12,28,43] The micromorphology was studied by high-resolution TEM (Figure 4a−f) and SEM (Figure 4g−l). The porous structures of **IMP-1−4** and **U-IMP-6** are directly visible by high-resolution TEM, reflecting their intrinsic porosity. The TEM image of **IMP-5** shows a layered-nanosheet arrangement and a nonporous structure. The SEM images of **IMP-1−4** and **U-IMP-6** reveal similar morphologies with aggregated clusters, coarse surfaces, and loosely structured irregular particles. Moreover, elemental mapping showed that carbon (C), nitrogen (N), oxygen (O), and iodine(I) for **IMP-4** (Figure S2) were distributed evenly throughout the material. The

Table 1. ICs, Porosity Parameters, and Adsorption Capacities toward Various Dyes of the Polymers in This Study

sample	IC (mmol g^{-1})	S_{BET} (m^2 g^{-1})[a]	V_{total} (cm^3 g^{-1})[b]	D_{aver} (nm)[c]	$AO7^-$ (mg g^{-1})	MB^{2-} (mg g^{-1})	AMR^{3-} (mg g^{-1})	MLB^+ (mg g^{-1})
IMP-1	1.32	71.4	0.40	22.4	276.3	24.5	102.5	1.0
IMP-2	1.30	113.4	0.48	16.8	366.5	29.9	154.6	4.1
IMP-3	1.15	78.3	0.51	26.0	249.9	18.1	46.1	1.0
IMP-4	1.55	74.2	0.52	28.0	559.4	32.6	203.8	1.0
IMP-5	1.55	2.2	0.01	12.6	10.5	3.6	8.0	3.2
U-IMP-6	0	74.0	0.38	20.4	26.1	17.0	5.2	4.9

[a]Surface area calculated from nitrogen adsorption isotherm at 77.3 K using the BET equation. [b]V_{total}: total pore volume calculated from nitrogen adsorption isotherm at P/P_0 = 0.99, 77.3 K. [c]D_{aver}: adsorption average pore diameter calculated by the BET method.

https://doi.org/10.1021/acs.macromol.2c01127
Macromolecules 2022, 55, 8784−8794

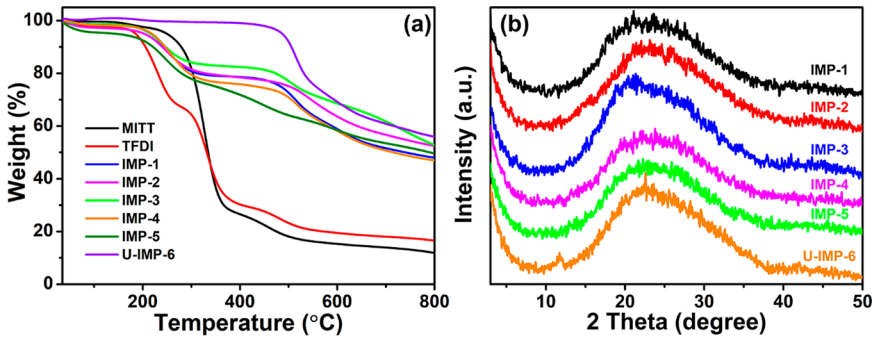

Figure 3. (a) TGA curves of the monomers (**MITT** and **TFDI**), imidazolium-based COPs (**IMP-1−5**) and uncharged polymer **U-IMP-6**. (b) PXRD profiles of **IMP-1−5** and **U-IMP-6**.

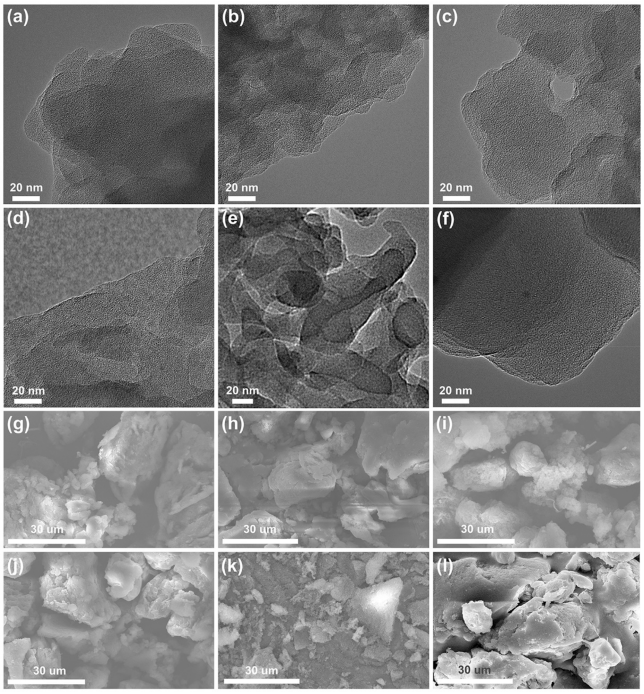

Figure 4. High-resolution TEM images of (a) **IMP-1**, (b) **IMP-2**, (c) **IMP-3**, (d) **IMP-4**, (e) **IMP-5**, and (f) **U-IMP-6** (the scale bars are insets). SEM images of (g) **IMP-1**, (h) **IMP-2**, (i) **IMP-3**, (j) **IMP-4**, (k) **IMP-5**, and (l) **U-IMP-6** (the scale bars are insets).

elemental mapping of iodine supports the presence of free iodide. The XPS data of **IMP-1−5** and **U-IMP-6** are listed in Table S2. The iodine content showed a good correlation with IC in **IMP-1−5**, while there was almost no iodine in **U-IMP-6**, indicating the successful preparation of the polymers.

Dye Adsorption by the Imidazolium-Based COPs. *Adsorption Capacities for Various Dyes.* Imidazolium-based COPs are stable and insoluble in common aqueous and organic reagents, which provides possibilities for removing hazardous organic dyes from wastewater. According to many reports, imidazolium-based COPs adsorb anionic dyes excellently.[12,50] In this study, we chose four organic dyes as model adsorbates with which the adsorption capacities of **IMP-1−5** and **U-IMP-6** were systematically studied (Figure 5 and Table 1). Among them, MLB^+ is a cationic dye, whereas $AO7^-$, MB^{2-}, and AMR^{3-} are anionic dyes with various charges and molecular sizes (Figure 5a).

Notably, **IMP-1−5** showed almost no ability to adsorb the cationic dye (MLB^+), which is ascribable to repulsion between the similarly charged cationic imidazolium and the cationic dye. On the other hand, **IMP-1−5** preferentially adsorbed the three anionic dyes ($AO7^-$, MB^{2-}, and AMR^{3-}) in the same order, namely $AO7^- > AMR^{3-} > MB^{2-}$. The observed trend is possibly ascribable to: (1) The molecular sizes of the dyes. According to DFT calculations (Table S3), $AO7^-$ is the smallest molecule in size, while MB^{2-} is the largest. Smaller dye molecules enter pores more easily to combine with adsorption sites. (2) Dye molecule charge. MB^{2-} and AMR^{3-} are doubly and triply negatively charged, respectively; hence, they are 2 and 3 times more able to counteract the charges on the imidazolium-based COP backbone than $AO7^-$, which reduces the number of effective adsorption sites and limits the improvement in adsorption capacity.

For the neutral uncharged **U-IMP-6**, the order of adsorption is $AO7^- > MB^{2-} > AMR^{3-}$. As the smallest molecule, $AO7^-$ easily enters the pores of **U-IMP-6**, so it is reasonable for its

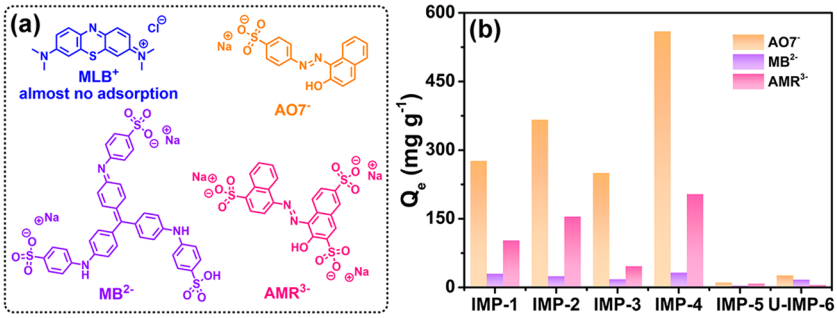

Figure 5. (a) Structures of MLB^+, $AO7^-$, MB^{2-}, and AMR^{3-}. (b) Histograms of the adsorption capacities of **IMP-1−5** and **U-IMP-6** for $AO7^-$, MB^{2-}, and AMR^{3-}.

https://doi.org/10.1021/acs.macromol.2c01127
Macromolecules 2022, 55, 8784−8794

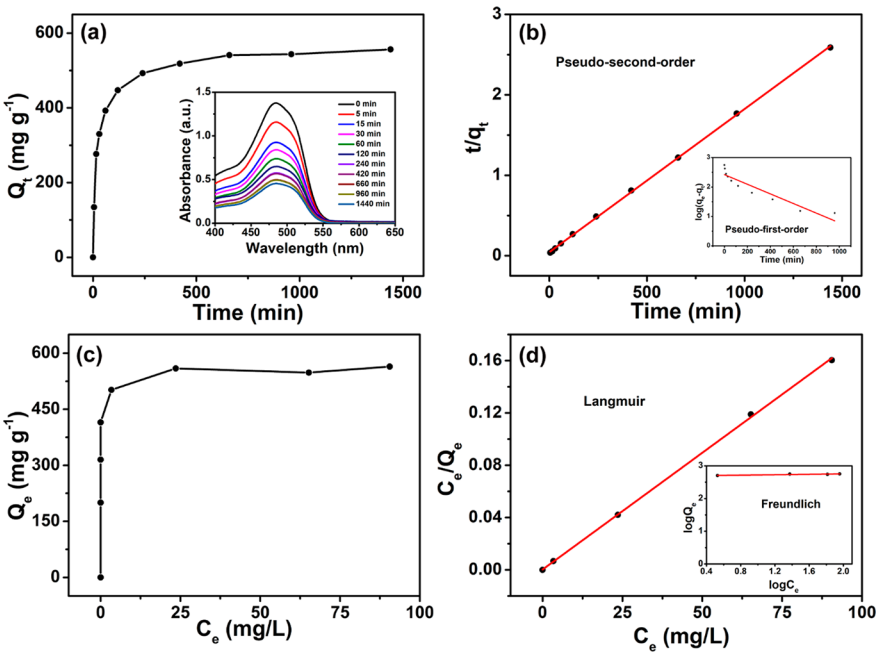

Figure 6. (a) Sorption kinetics data of **IMP-4** for $AO7^-$. (b) Fitted $AO7^-$ kinetic data for adsorption by **IMP-4**. (c) Sorption isotherm for $AO7^-$ on **IMP-4**. (d) Fitted $AO7^-$ isotherm data for adsorption by **IMP-4**.

highest adsorption capacity. Compared with the methylated imidazolium cation rings in **IMP-1−5**, the uncharged imidazole ring in **U-IMP-6** contains a N atom with a lone pair of electrons, which can form strong hydrogen bonds with two −NH− groups and a sulfonic acid group in MB^{2-}. Therefore, **U-IMP-6** is more effective in the adsorption of MB^{2-} than AMR^{3-} which only contains one −OH group.

We next thoroughly analyzed how IC and porosity specifically influence adsorption performance. Given that imidazolium-based COPs exhibit similar adsorption trends for the anionic dyes ($AO7^-$, MB^{2-}, and AMR^{3-}), we chose $AO7^-$ as an illustrative example. As summarized in Table 1, **IMP-2** has a similar IC but a much higher BET surface (113.4 vs 71.4 $m^2\ g^{-1}$) than **IMP-1**, and its adsorption capacity is higher than that of **IMP-1**, which indicates that higher porosity beneficially provides more dye-adsorption sites. On the other hand, **IMP-3** has a similar surface area to **IMP-1** but a lower IC (1.15 vs 1.32 mmol g^{-1}); hence, its $AO7^-$ adsorption capacity is lower than that of **IMP-1**. Here, we verify the important role that IC plays in adsorption; that is, more charges effectively strengthen the electrostatic interactions between the polymer and dye molecules. **IMP-4**, with the shortest repeating unit, was prepared to further increase the IC; its surface area was maintained at a level similar to those of **IMP-1** and **IMP-3**, and notably, it exhibited a significantly higher adsorption capacity because of its higher IC (1.55 mmol g^{-1}), which is even higher than that of **IMP-2** (with the highest surface area of 113.4 $m^2\ g^{-1}$). This finding suggests that increasing the charge content is very useful for enhancing dye removal, even more effective than increasing the surface area.

IMP-5 is composed of the same reactive monomer as **IMP-4** and therefore has the same theoretical IC; however, it showed almost no dye-adsorbing ability, which suggests that pores provide essential adsorption sites for dye molecules. Even a polymer with a high charge content cannot adsorb in the absence of pores. **U-IMP-6** is uncharged and therefore has an IC of 0 mmol g^{-1}. Despite having a surface area comparable to that of **IMP-4** (74.0 vs 74.2 $m^2\ g^{-1}$), its adsorption capacity for $AO7^-$ is significantly lower (26.1 vs 559.4 mg g^{-1}), which suggests that electrostatic interactions between the cationic host polymer and guest molecules play dominant roles in promoting highly efficient dye adsorption.

Besides the BET specific surface area, PSD, pore size, and pore volume are also important parameters affecting adsorption. As reported previously, the hierarchical pore structure and relatively large pore size were deemed beneficial to the mass flow and access to the cationic active sites for dyes.[12] Moreover, the pore volume is vital in providing enough space for dye molecules and achieving high adsorption capacity.[51] For instance, the ICs of **IMP-3**, **IMP-1**, and **IMP-4** increased by 1.15, 1.32, and 1.55 mmol g^{-1}, respectively, and their adsorption capacities increase by 249.9, 276.3, and 559.4 mg g^{-1}, respectively. **IMP-4** has a remarkably high adsorption capacity compared to the others. In addition to the higher IC leading to the enhancement of the electrostatic interaction between the skeleton and the guest dye molecules, it may be also related to its PSD, pore volume, and pore size. For example, compared with **IMP-1** and **IMP-3**, the pores in **IMP-4** fit a normal distribution (Figure 2b). Moreover, **IMP-4** has a larger pore size and pore volume (Table 1), which is also conducive to dye molecules entering the pore and providing sufficient space for adsorption. Therefore, the remarkably high adsorption capacity could derive from the synergy of the IC and porosity.

In summary, the above results are complementary in that they fully confirm that porosity is the basis for a high organic-dye adsorption capacity, while electrostatic interactions derived from the positively charged groups within the polymer backbone are the dominant forces that drive efficient dye removal; increasing the charge content was found to be more effective at improving adsorption performance than increasing the surface area in this polymer system. Here, we reveal that synergy between the IC and porosity of the adsorbent contributes significantly to dye-adsorption capacity, which

https://doi.org/10.1021/acs.macromol.2c01127
Macromolecules 2022, 55, 8784−8794

may be equally applicable to other anionic contaminants in water.

Adsorption Kinetics and Isotherms. We studied the kinetic and adsorption-isotherm behavior of **IMP-4** (5 mg) toward $AO7^-$ (25 mL, 160 mg L^{-1}) because this adsorbent exhibited the highest adsorption capacity. Figure 6a shows the relationship between $AO7^-$ uptake and adsorption time by **IMP-4**, which was determined by monitoring the $AO7^-$ solution concentration over time. The intensity of the characteristic peak at 484 nm in the UV−vis spectrum of $AO7^-$ decreased rapidly over 60 min (Figure 6a, inset), and the adsorption capacity was calculated to be 392.5 mg g^{-1} based on eq 1 in the Supporting Information, with a removal efficiency of 49.4% (eq 2 in the Supporting Information). Stable adsorption equilibrium was achieved after 1440 min. The comparison of maximum adsorption capacities of **IMP-4** and other reported COPs adsorbents for $AO7^-$ are summarized in Table 2. The maximum adsorption capacity of **IMP-4** is similar to the reported imidazolium-based COP ImPOP-1 by Han et al. and higher than most of the reported COPs materials in Table 2, indicating the advantage of imidazolium-based cationic organic polymers in efficient dye adsorption.

Table 2. Comparison of Maximum Adsorption Capacities (q_{max}) of Various COPs Adsorbents Reported in the Literature for $AO7^-$ Dye Adsorption

adsorbents	adsorption capacity (mg g^{-1})	ref
IMP-4	559.4	this work
zerovalent Fe NPs	66.6	5
ImPOP-1	578.5	12
QPSP	215.5	52
MIL-100 (Fe)	409.8	53
CMs4	218.6	54

We next fitted the fast adsorption kinetics data to the pseudo-first-order and pseudo-second-order kinetic models, with Figure 6b revealing that the adsorption process is well fitted by the pseudo-second-order kinetic model ($R^2 > 0.999$), which indicates that the $AO7^-$-adsorption rate on **IMP-4** depends on the availability of active sites.

The **IMP-4** adsorption isotherm was acquired to further understand its adsorption properties (Figure 6c). Notably, the amount of $AO7^-$ adsorbed increased almost linearly with increasing initial $AO7^-$ concentration at $AO7^-$ concentrations less than 160 mg L^{-1}, which is attributable to the fact that **IMP-4** is capable of providing sufficient active adsorption sites for $AO7^-$ molecules at low concentrations. Most active adsorption sites became occupied during the initial stage as the initial $AO7^-$ concentration was further increased, resulting in a gradual decline in the adsorption rate as equilibrium was approaching.

The isotherm data were fitted to the widely used Langmuir and Freundlich isotherm models (Figure 6d and Table S5). According to the curves of best fit and the observed correlation, the isotherm data are better described by the Langmuir model ($R^2 > 0.999$), which indicates that the $AO7^-$ dye is adsorbed on the **IMP-4** surface in a monolayer process.

Adsorption Selectivity. The adsorption selectivity of a material is one of the most important factors for water treatment applications. Cationic and anionic organic dyes often coexist in wastewater from textile-related industries; therefore, separating these differently charged dyes is an important water-treatment objective. Herein, we investigated whether or not imidazolium-based COPs are capable of selectively removing a target anionic dye in the presence of an interfering dye. We used an $AO7^-/MLB^+$ mixed-dye solution for separation testing. A dark brown mixture was formed when $AO7^-$ was mixed with the oppositely charged MLB^+ (Figure 7, inset).

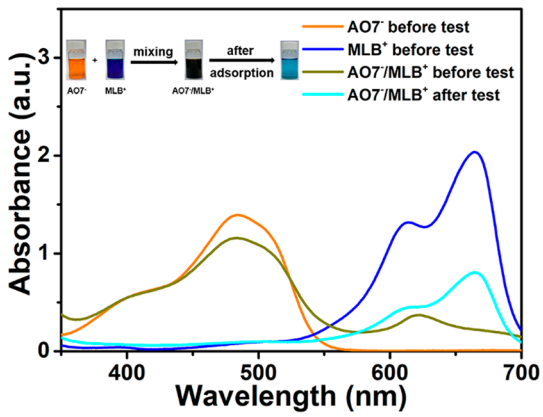

Figure 7. Selectivity performance of **IMP-4** determines by solution adsorption testing. The UV−vis spectra of $AO7^-$ (160 mg L^{-1}), MLB^+ (45 mg L^{-1}), and the mixture $AO7^-/MLB^+$ before and after adsorption. The inset shows digital photographs of the dye solution ($AO7^-$ and MLB^+ solutions, $AO7^-/MLB^+$ mixture before and after separation).

Notably, the peak intensity of $AO7^-$ and MLB^+ weakened obviously in the UV spectra after mixing, resulting from a complex formation of two oppositely charged dyes in the mixing solution.[12] **IMP-4** was then added to the dye mixture and filtered after stirring for 24 h. The color of $AO7^-/MLB^+$ mixture changed from dark brown to blue, indicative of the successful separation of the two oppositely charged molecules. The separation efficiency was further determined by UV−vis spectroscopy, which revealed that the anionic $AO7^-$ dye was almost completely removed, as evidenced by the dramatic decrease in the intensity of the spectral peak at ∼484 nm, as shown in Figure 7. At the same time, an increase in the MLB^+ peak was also observed because most of the complex decomposed to release MLB^+ molecules after selective adsorption of the $AO7^-$ molecules by **IMP-4**. However, the intensity of the peak of MLB^+ is still lower than its original state, which may be due to part of MLB^+ combined with $AO7^-$ as the complex and simultaneously absorbed by **IMP-4**. This phenomenon also appeared in a similar adsorption selectivity study.[12] In brief, this binary-mixture study revealed that the adsorption of the target anionic dye was substantially unaffected by the presence of an interfering dye.

Recyclability Test. In this study, $AO7^-$ was chosen as a model dye to investigate the recyclability of **IMP-4**. We employed a mixture of MeOH and saturated NaCl aqueous in the ratio of 10:1 (v:v) to regenerate **IMP-4** because saturated NaCl aqueous solution is beneficial for exchanging the $AO7^-$ anions, and MeOH can decrease the interaction between **IMP-4** and $AO7^-$. As a result, $AO7^-$ got desorbed from **IMP-4**. The adsorption−desorption cycle test was performed for consecutive five cycles. As shown in Figure 8a, the adsorption capacities of $AO7^-$ decrease from 559.4 to 443.3 mg g^{-1} after five cycles, with the removal efficiencies decreasing from 87.8 to 68.7%. The gradual drop of adsorption capacity in the cycles

https://doi.org/10.1021/acs.macromol.2c01127
Macromolecules 2022, 55, 8784−8794

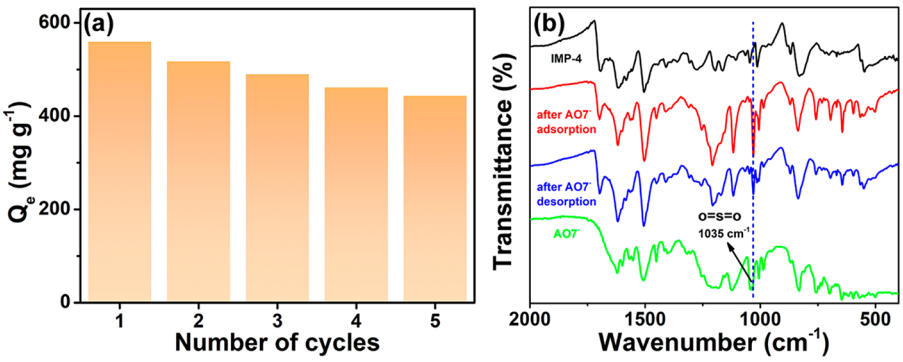

Figure 8. (a) Reusability of **IMP-4** for AO7$^-$. (b) FTIR spectra of **IMP-4**, **IMP-4** after AO7$^-$ adsorption, **IMP-4** after AO7$^-$ desorption, and AO7$^-$.

might be due to the blockage of the active sites by AO7$^-$ molecules because of the strong electrostatic interactions between the imidazolium cations in **IMP-4** and SO_3^- group in AO7$^-$. The contrast of the FTIR spectra of the original **IMP-4**, the **IMP-4** after AO7$^-$ adsorption, the **IMP-4** after AO7$^-$ desorption, and the AO7$^-$ is shown in Figure 8b. After the adsorption of AO7$^-$ into the **IMP-4**, a characteristic peak appeared at 1035 cm^{-1} attributable to the O═S═O stretching from AO7$^-$. After the desorption of AO7$^-$, the greatly weakened band at 1035 cm^{-1} was observed, further indicating the incomplete desorption, which is also the reason for the decrease of the adsorption capacity in the recyclability test.

CONCLUSIONS

A series of novel imidazolium-based COPs were designed and prepared using Schiff-base chemistry. IC and porosity were regulated by adjusting the structures of the building units. The charge-incorporated polymer without pores was almost incapable of adsorbing dyes. Among polymers with similar porosities, COPs with higher IC values exhibited higher adsorption capacities, and the polymer **IMP-4** with the largest IC but only a surface area of 74.2 m^2 g^{-1} exhibited the best adsorption performance toward AO7$^-$ (559.4 mg g^{-1}, 21 times that of the uncharged **U-IMP-6**). The results demonstrated that synergy between IC and intrinsic porosity impacts the effectiveness of the adsorption process; i.e., high porosity is the basis of high adsorption capacity toward organic dyes, while electrostatic interactions between structural charges and dyes are the dominant driving forces for organic-dye adsorption. Hence, increasing the charge content is expected to be a more effective strategy to improve adsorption than increasing the surface area. This study sheds light on the understanding of the adsorption process of the organic dyes, which would provide key guidance on the further development of ionic porous adsorbents for wastewater treatment.

ASSOCIATED CONTENT

Supporting Information

The Supporting Information is available free of charge at https://pubs.acs.org/doi/10.1021/acs.macromol.2c01127.

Synthesis procedure of 2,4,5-tribromo-1-methyl-1*H*-imidazole, ^{1}H NMR, ^{13}C NMR, and high-resolution mass spectra of small molecules, sorption kinetics study, sorption isotherm study, adsorption tests for different dyes, dye separation test, recyclability test, and density functional theory calculations (PDF)

AUTHOR INFORMATION

Corresponding Authors

Pei-Nian Liu − *Shanghai Key Laboratory of Functional Materials Chemistry, Key Laboratory for Advanced Materials and School of Chemistry and Molecular Engineering, East China University of Science and Technology, Shanghai 200237, China;* orcid.org/0000-0003-2014-2244; Email: liupn@ecust.edu.cn

Boxin Xue − *Shanghai Key Laboratory of Functional Materials Chemistry, Key Laboratory for Advanced Materials and School of Chemistry and Molecular Engineering, East China University of Science and Technology, Shanghai 200237, China*; Email: bxxue@ecust.edu.cn

Authors

Shu-Qing Fu − *Shanghai Key Laboratory of Functional Materials Chemistry, Key Laboratory for Advanced Materials and School of Chemistry and Molecular Engineering, East China University of Science and Technology, Shanghai 200237, China*

Ming-Zhi Zhu − *Shanghai Key Laboratory of Functional Materials Chemistry, Key Laboratory for Advanced Materials and School of Chemistry and Molecular Engineering, East China University of Science and Technology, Shanghai 200237, China*

Complete contact information is available at: https://pubs.acs.org/10.1021/acs.macromol.2c01127

Notes

The authors declare no competing financial interest.

ACKNOWLEDGMENTS

This work was supported by the National Natural Science Foundation of China (Nos. 21925201 and 22161160319), the Shanghai Sailing Program (21YF1409300), the China Postdoctoral Science Foundation (2021M691007), the Program for Eastern Scholar Distinguished Professor, and the Fundamental Research Funds for the Central Universities. We thank the Research Center of Analysis and Test of East China University of Science and Technology for help in the characterization.

REFERENCES

(1) Watharkar, A. D.; Kadam, S. K.; Khandare, R. V.; Kolekar, P. D.; Jeon, B. H.; Jadhav, J. P.; Govindwar, S. P. Asparagus Densiflorus in a Vertical Subsurface Flow Phytoreactor for Treatment of Real Textile Effluent: A lab to Land Approach for in Situ Soil Remediation. *Ecotoxicol. Environ. Saf* **2018**, *161*, 70−77.

(2) Shen, X.; Faheem, M.; Matsuo, Y.; Aziz, S.; Zhang, X.; Li, Y.; Song, J.; Tian, Y.; Zhu, G. Polarity Engineering of Porous Aromatic Frameworks for Specific Water Contaminant Capture. *J. Mater. Chem. A* **2019**, *7*, 2507−2512.
(3) Alsbaiee, A.; Smith, B. J.; Xiao, L.; Ling, Y.; Helbling, D. E.; Dichtel, W. R. Rapid Removal of Organic Micropollutants from Water by a Porous β-Cyclodextrin Polymer. *Nature* **2016**, *529*, 190−194.
(4) Xue, H.; Wang, X.; Xu, Q.; Dhaouadi, F.; Sellaoui, L.; Seliem, M. K.; Lamine, A. B.; Belmabrouk, H.; Bajahzar, A.; Bonilla-Petriciolet, A.; Li, Z.; Li, Q. Adsorption of Methylene Blue from Aqueous Solution on Activated Carbons and Composite Prepared from an Agricultural Waste Biomass: A Comparative Study by Experimental and Advanced Modeling Analysis. *Chem. Eng. J.* **2022**, *430*, 132801.
(5) Zaheer, Z.; Bawazir, W. A.; Al-Bukhari, S. M.; Basaleh, A. S. Adsorption, Equilibrium Isotherm, and Thermodynamic Studies to the Removal of Acid Orange 7. *Mater. Chem. Phys.* **2019**, *232*, 109−120.
(6) Rodrigues, F. K.; Salau, N. P. G.; Dotto, G. L. New Insights about Reactive Red 141 Adsorption onto Multi-walled Carbon Nanotubes Using Statistical Physics Coupled with Van der Waals Equation. *Sep. Purif. Technol.* **2019**, *224*, 290−294.
(7) Rafatullah, M.; Sulaiman, O.; Hashim, R.; Ahmad, A. Adsorption of Methylene Blue on Low-Cost Adsorbents: A Review. *J. Hazard. Mater.* **2010**, *177*, 70−80.
(8) Wang, B.; Xie, Z.; Li, Y.; Yang, Z.; Chen, L. Dual-Functional Conjugated Nanoporous Polymers for Efficient Organic Pollutants Treatment in Water: A Synergistic Strategy of Adsorption and Photocatalysis. *Macromolecules* **2018**, *51*, 3443−3449.
(9) Yuan, Y.; Huang, H.; Chen, L.; Chen, Y. N,N′-Bicarbazole: A Versatile Building Block toward the Construction of Conjugated Porous Polymers for CO_2 Capture and Dyes Adsorption. *Macromolecules* **2017**, *50*, 4993−5003.
(10) Gao, W.; Tian, J.; Fang, Y.; Liu, T.; Zhang, X.; Xu, X.; Zhang, X. Visible-Light-Driven Photo-Fenton Degradation of Organic Pollutants by a Novel Porphyrin-Based Porous Organic Polymer at Neutral pH. *Chemosphere* **2020**, *243*, 125334.
(11) Huang, M.; Yang, L.; Li, X.; Chang, G. An Indole-Derived Porous Organic Polymer for the Efficient Visual Colorimetric Capture of Iodine in Aqueous Media via the Synergistic Effects of Cation-π and Electrostatic Forces. *Chem. Commun.* **2020**, *56*, 1401−1404.
(12) Liu, Z.-W.; Cao, C.-X.; Han, B.-H. A Cationic Porous Organic Polymer for High-Capacity, Fast, and Selective Capture of Anionic Pollutants. *J. Hazard. Mater.* **2019**, *367*, 348−355.
(13) Yang, X.-Y.; Chen, L.-H.; Li, Y.; Rooke, J. C.; Sanchez, C.; Su, B.-L. Hierarchically Porous Materials: Synthesis Strategies and Structure Design. *Chem. Soc. Rev.* **2017**, *46*, 481−558.
(14) Aguila, B.; Sun, Q.; Perman, J. A.; Earl, L. D.; Abney, C. W.; Elzein, R.; Schlaf, R.; Ma, S. Efficient Mercury Capture Using Functionalized Porous Organic Polymer. *Adv. Mater.* **2017**, *29*, 1700665.
(15) Sun, Q.; Zhu, L.; Aguila, B.; Thallapally, P. K.; Xu, C.; Chen, J.; Wang, S.; Rogers, D.; Ma, S. Optimizing Radionuclide Sequestration in Anion Nanotraps with Record Pertechnetate Sorption. *Nat. Commun.* **2019**, *10*, 1646.
(16) Rivero-Crespo, M. A.; Toupalas, G.; Morandi, B. Preparation of Recyclable and Versatile Porous Poly(aryl thioether)s by Reversible Pd-Catalyzed C-S/C-S Metathesis. *J. Am. Chem. Soc.* **2021**, *143*, 21331−21339.
(17) Qian, X.; Zhu, Z.-Q.; Sun, H.-X.; Ren, F.; Mu, P.; Liang, W.; Chen, L.; Li, A. Capture and Reversible Storage of Volatile Iodine by Novel Conjugated Microporous Polymers Containing Thiophene Units. *ACS Appl. Mater. Interfaces* **2016**, *8*, 21063−21069.
(18) Zhang, L.; Sun, J.-S.; Sun, F.; Chen, P.; Liu, J.; Zhu, G. Facile Synthesis of Ultrastable Porous Aromatic Frameworks by Suzuki-Miyaura Coupling Reaction for Adsorption Removal of Organic Dyes. *Chem.—Eur. J.* **2019**, *25*, 3903−3908.
(19) Zhao, R.; Ma, T.; Cui, F.; Tian, Y.; Zhu, G. Porous Aromatic Framework with Tailored Binding Sites and Pore Sizes as a High-Performance Hemoperfusion Adsorbent for Bilirubin Removal. *Adv. Sci.* **2020**, *7*, 2001899.
(20) Abubakar, S.; Skorjanc, T.; Shetty, D.; Trabolsi, A. Porous Polycalix[*n*]arenes as Environmental Pollutant Removers. *ACS Appl. Mater. Interfaces* **2021**, *13*, 14802−14815.
(21) Kong, H.-Y.; Wang, T.-X.; Tao, Y.; Ding, X.; Han, B.-H. Crown Ether-Based Hypercrosslinked Porous Polymers for Gold Adsorption. *Sep. Purif. Technol.* **2022**, *290*, 120805.
(22) Huang, X.-Q.; Hong, X.; Lin, H.; Cao, X.-M.; Dang, Q.; Tang, S.-B.; Chen, D.-L.; Zhang, Y. Hypercrosslinked Triazine-Phloroglucinol Hierarchical Porous Polymers for the Effective Removal of Organic Micropollutants. *Chem. Eng. J.* **2022**, *435*, 134990.
(23) Cucu, E.; Dalkilic, E.; Altundas, R.; Sadak, A. E. Gas Sorption and Selectivity Study of *N,N,N′,N′*-Tetraphenyl-1,4-phenylenediamine Based Microporous Hyper-Crosslinked Polymers. *Microporous Mesoporous Mater.* **2022**, *330*, 111567.
(24) Ravi, S.; Kim, S.-Y.; Bae, Y.-S. Novel Benzylphosphate-Based Covalent Porous Organic Polymers for the Effective Capture of Rare Earth Elements from Aqueous Solutions. *J. Hazard. Mater.* **2022**, *424*, 127356.
(25) Giri, A.; Biswas, S.; Hussain, MD. W.; Dutta, T. K.; Patra, A. Nanostructured Hypercrosslinked Porous Organic Polymers: Morphological Evolution and Rapid Separation of Polar Organic Micropollutants. *ACS Appl. Mater. Interfaces* **2022**, *14*, 7369−7381.
(26) Zhang, C.; Zhu, P.-C.; Tan, L.; Liu, J.-M.; Tan, B.; Yang, X.-L.; Xu, H.-B. Triptycene-Based Hyper-Cross-Linked Polymer Sponge for Gas Storage and Water Treatment. *Macromolecules* **2015**, *48*, 8509−8514.
(27) Liu, M.; Li, M.; Jiang, Y.; Ma, Z.; Liu, D.; Ren, Z.; Russell, T. P.; Liu, Y. Conductive Ionenes Promote Interfacial Self-Doping for Efficient Organic Solar Cells. *ACS Appl. Mater. Interfaces* **2021**, *13*, 41810−41817.
(28) Hu, Q.-H.; Jiang, W.; Liang, R.-P.; Lin, S.; Qiu, J.-D. Synthesis of Imidazolium-Based Cationic Organic Polymer for Highly Efficient and Selective Removal of ReO_4^-/TcO_4^-. *Chem. Eng. J.* **2021**, *419*, 129546.
(29) Sen, A.; Dutta, S.; Dam, G. K.; Samanta, P.; Let, S.; Sharma, S.; Shirolkar, M. M.; Ghosh, S. K. Imidazolium-Functionalized Chemically Robust Ionic Porous Organic Polymers (*i*POPs) toward Toxic Oxo-Pollutants Capture from Water. *Chem.—Eur. J.* **2021**, *27*, 13442−13449.
(30) Li, J.; Dai, X.; Zhu, L.; Xu, C.; Zhang, D.; Silver, M. A.; Li, P.; Chen, L.; Li, Y.; Zuo, D.; Zhang, H.; Xiao, C.; Chen, J.; Diwu, J.; Farha, O. K.; Albrecht-Schmitt, T. E.; Chai, Z.; Wang, S. $^{99}TcO_4^-$ Remediation by a Cationic Polymeric Network. *Nat. Commun.* **2018**, *9*, 3007.
(31) Mandal, W.; Fajal, S.; Mollick, S.; Shirolkar, M. M.; More, Y. D.; Saurabh, S.; Mahato, D.; Ghosh, S. K. Unveiling the Impact of Diverse Morphology of Ionic Porous Organic Polymers with Mechanistic Insight on the Ultrafast and Selective Removal of Toxic Pollutants from Water. *ACS Appl. Mater. Interfaces* **2022**, *14*, 20042−20052.
(32) Mu, Z.; Zhu, Y.; Li, B.; Dong, A.; Wang, B.; Feng, X. Covalent Organic Frameworks with Record Pore Apertures. *J. Am. Chem. Soc.* **2022**, *144*, 5145−5154.
(33) Pan, F.; Guo, W.; Su, Y.; Khan, N. A.; Yang, H.; Jiang, Z. Direct Growth of Covalent Organic Framework Nanofiltration Membranes on Modified Porous Substrates for Dyes Separation. *Sep. Purif. Technol.* **2019**, *215*, 582−589.
(34) Gomes, R.; Bhanja, P.; Bhaumik, A. A Triazine-Based Covalent Organic Polymer for Efficient CO_2 Adsorption. *Chem. Commun.* **2015**, *51*, 10050−10053.
(35) Da, H.-J.; Yang, C.-X.; Yan, X.-P. Cationic Covalent Organic Nanosheets for Rapid and Selective Capture of Perrhenate: An Analogue of Radioactive Pertechnetate from Aqueous Solution. *Environ. Sci. Technol.* **2019**, *53*, 5212−5220.
(36) Xiong, G.; Wang, B.-B.; You, L.-X.; Ren, B.-Y.; He, Y.-K.; Ding, F.; Dragutan, I.; Dragutan, V.; Sun, Y.-G. Hypervalent Silicon-Based, Anionic Porous Organic Polymers with Solid Microsphere or Hollow

https://doi.org/10.1021/acs.macromol.2c01127
Macromolecules 2022, 55, 8784−8794

Nanotube Morphologies and Exceptional Capacity for Selective Adsorption of Cationic Dyes. *J. Mater. Chem. A* **2019**, *7*, 393−404.
(37) Jiao, S.; Deng, L.; Zhang, X.; Zhang, Y.; Liu, K.; Li, S.; Wang, L.; Ma, D. Evaluation of an Ionic Porous Organic Polymer for Water Remediation. *ACS Appl. Mater. Interfaces* **2021**, *13*, 39404−39413.
(38) Wang, Y.; Xie, Y.; Zhang, Y.; Tang, S.; Guo, C.; Wu, J.; Lau, R. Anionic and Cationic Dyes Adsorption on Porous Poly-Melamine-Formaldehyde Polymer. *Chem. Eng. Res. Des.* **2016**, *114*, 258−267.
(39) Fu, H.-R.; Xu, Z.-X.; Zhang, J. Water-Stable Metal-Organic Frameworks for Fast and High Dichromate Trapping via Single-Crystal-to-Single-Crystal Ion Exchange. *Chem. Mater.* **2015**, *27*, 205−210.
(40) Mei, L.; Li, F.-Z.; Lan, J.-H.; Wang, C.-Z.; Xu, C.; Deng, H.; Wu, Q.-Y.; Hu, K.-Q.; Wang, L.; Chai, Z.-F.; Chen, J.; Gibson, J. K.; Shi, W.-Q. Anion-Adaptive Crystalline Cationic Material for $^{99}TcO_4^-$ Trapping. *Nat. Commun.* **2019**, *10*, 1532.
(41) Chen, Y.; Li, Z.; Ding, R.; Liu, T.; Zhao, H.; Zhang, X. Construction of Porphyrin and Viologen-Linked Cationic Porous Organic Polymer for Efficient and Selective Gold Recovery. *J. Hazard. Mater.* **2022**, *426*, 128073.
(42) Yu, S.-B.; Lyu, H.; Tian, J.; Wang, H.; Zhang, D.-W.; Liu, Y.; Li, Z.-T. A Polycationic Covalent Organic Framework: A Robust Adsorbent for Anionic Dye Pollutants. *Polym. Chem.* **2016**, *7*, 3392−3397.
(43) Ding, M.; Chen, L.; Xu, Y.; Chen, B.; Ding, J.; Wu, R.; Huang, C.; He, Y.; Jin, Y.; Xia, C. Efficient Capture of Tc/Re(VII, IV) by a Viologen-Based Organic Polymer Containing Tetraaza Macrocycles. *Chem. Eng. J.* **2020**, *380*, 122581.
(44) Liu, Z.-W.; Han, B.-H. Evaluation of an Imidazolium-Based Porous Organic Polymer as Radioactive Waste Scavenger. *Environ. Sci. Technol.* **2020**, *54*, 216−224.
(45) Huang, N.; Wang, P.; Addicoat, M. A.; Heine, T.; Jiang, D. Ionic Covalent Organic Frameworks: Design of a Charged Interface Aligned on 1D Channel Walls and Its Unusual Electrostatic Functions. *Angew. Chem. Int. Ed* **2017**, *56*, 4982−4986.
(46) Sana, B.; Das, A.; Jana, T. Cross-Linked Polybenzimidazoles as Alkaline Stable Anion Exchange Membranes. *ACS Appl. Energy Mater.* **2022**, *5*, 3626−3637.
(47) Evans, A. M.; Parent, L. R.; Flanders, N. C.; Bisbey, R. P.; Vitaku, E.; Kirschner, M. S.; Schaller, R. D.; Chen, L. X.; Gianneschi, N. C.; Dichtel, W. R. Seeded Growth of Single-Crystal Two-Dimensional Covalent Organic Frameworks. *Science* **2018**, *361*, 52−57.
(48) Smith, B. J.; Dichtel, W. R. Mechanistic Studies of Two-Dimensional Covalent Organic Frameworks Rapidly Polymerized from Initially Homogeneous Conditions. *J. Am. Chem. Soc.* **2014**, *136*, 8783−8789.
(49) Smith, B. J.; Parent, L. R.; Overholts, A. C.; Beaucage, P. A.; Bisbey, R. P.; Chavez, A. D.; Hwang, N.; Park, C.; Evans, A. M.; Gianneschi, N. C.; Dichtel, W. R. Colloidal Covalent Organic Frameworks. *ACS Cent. Sci.* **2017**, *3*, 58−65.
(50) Lin, J.; Su, T.; Chen, J.; Xue, T.; Yang, S.; Guo, P.; Lin, H.; Wang, H.; Hong, Y.; Su, Y.; Peng, L.; Li, J. Efficient Adsorption Removal of Anionic Dyes by an Imidazolium-Based Mesoporous Poly(ionic liquid) including the Continuous Column Adsorption-Desorption Process. *Chemosphere* **2021**, *272*, 129640.
(51) Parker, H. L.; Hunt, A. J.; Budarin, V. L.; Shuttleworth, P. S.; Miller, K. L.; Clark, J. H. The Importance of Being Porous: Polysaccharide-derived Mesoporous Materials for Use in Dye Adsorption. *RSC Adv.* **2012**, *2*, 8992−8997.
(52) Kaya, A.; Sahin, S. A. Acid Orange 7 Adsorption onto Quaternized Pistachio Shell Powder from Aqueous Solutions *Biomass Convers. Biorefin*, 2022; DOI: 10.1007/s13399-022-02414-3.
(53) Tsai, F.-C.; Xia, Y.; Ma, N.; Shi, J.-J.; Jiang, T.; Chiang, T.-C.; Zhang, Z.-C.; Tsen, W.-C. Adsorptive Removal of Acid Orange 7 from Aqueous Solution with Metal-Organic Framework Material, Iron (III) Trimesate. *Desalin. Water Treat* **2016**, *57*, 3218−3226.
(54) Wan, Y.; Liu, Z.-Y.; Song, P.; Zhang, X.-Q.; Song, J.-C.; Fu, Y.-J.; Yao, X.-H.; Wang, J.; Chen, T.; Zhang, D.-Y.; Li, L.; Shi, C.-Y. Ionic Liquid Groups Modified 3D Porous Cellulose Microspheres for Selective Adsorption of AO7 Dye. *J. Cleaner Prod* **2019**, *240*, 118201.

https://doi.org/10.1021/acs.macromol.2c01127
Macromolecules 2022, 55, 8784−8794